JCI The Journal of Clinical Investigation

Expansion of hedgehog disrupts mesenchymal identity and induces emphysema phenotype

Chaoqun Wang, … , Harold A. Chapman, Tien Peng

J Clin Invest. 2018. https://doi.org/10.1172/JCI99435.

Research In-Press Preview **Development** **Pulmonology**

Graphical abstract

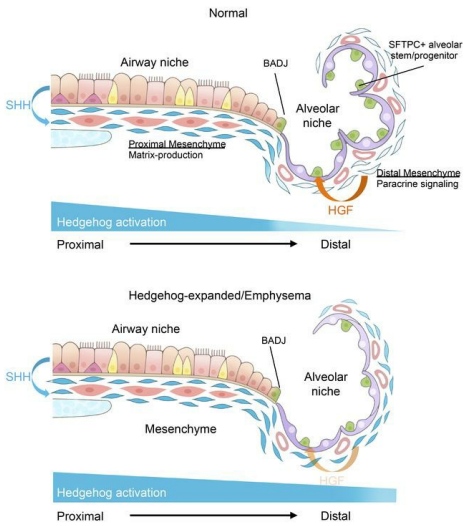

Title

Expansion of hedgehog disrupts mesenchymal identity and induces emphysema phenotype

Authors
Chaoqun Wang[1], Nabora S. Reyes de Mochel[1], Stephanie A. Christenson[1], Monica Cassandras[1], Rebecca Moon[1], Alexis N. Brumwell[1], Lauren E. Byrnes[2], Alfred Li[3], Yasuyuki Yokosaki[4], Peiying Shan[5], Julie B. Sneddon[2], David Jablons[6], Patty J. Lee[5], Michael A. Matthay[1], Hal A. Chapman[1], and Tien Peng[1,7*]

[1]Department of Medicine
[2]Diabetes Center
[3]Bone Imaging Research Core
[6]Department of Surgery
[7]Cardiovascular Research Institute
University of California San Francisco
San Francisco, CA 94143

[4]Hiroshima University
Hiroshima, Japan

[5]Yale School of Medicine
New Haven, CT

*Address correspondence to:
Tien Peng, M.D.
University of California, San Francisco
513 Parnassus Ave.
HSE Building, Room 1312, Box 0130
San Francisco, CA 94143
Phone: 1-415-514-4180
Email: tien.peng@ucsf.edu

Conflict of interest statement:
The authors have declared that no conflict of interest exists.

Abstract

Genome-wide association studies have repeatedly mapped susceptibility loci for emphysema to genes that modify hedgehog signaling, but the functional relevance of hedgehog signaling to this morbid disease remains unclear. In the current study, we identified a broad population of mesenchymal cells in the adult murine lung receptive to hedgehog signaling, characterized by higher activation of hedgehog surrounding the proximal airway relative to the distal alveoli. Single cell RNA-sequencing showed that the hedgehog-receptive mesenchyme is composed of mostly fibroblasts with distinct proximal and distal subsets with discrete identities. Ectopic hedgehog activation in the distal fibroblasts promoted expression of proximal fibroblast markers, and promoted loss of distal alveoli and airspace enlargement of over twenty percent compared to controls. We found that hedgehog suppressed mesenchymal-derived mitogens enriched in distal fibroblasts that regulate alveolar stem cell regeneration and airspace size. Finally, single cell analysis of the human lung mesenchyme showed that segregated proximal-distal identity with preferential hedgehog activation in the proximal fibroblasts is conserved between mice and humans. In conclusion, we showed that differential hedgehog activation segregates mesenchymal identities of distinct fibroblast subsets, and disruption of fibroblast identity can alter the alveolar stem cell niche leading to emphysematous changes in the murine lung.

Introduction

Emphysema is a major subtype of chronic obstructive pulmonary disease (COPD) linked to tobacco exposure, and characterized by progressive loss of alveolar gas exchange surface and enlargement of distal airspace resulting from the loss of septated alveolar tissue (1). However, the observation that only a small subset of smokers eventually develops emphysema gave rationale to explore inherent genetic variations that confer susceptibility to this disease (2). Decades of research on emphysema pathogenesis have implicated diverse processes such as inflammation, protease imbalance, apoptosis, autophagy, oxidative stress, and *etc.* (3). However, recent large genome-wide association studies (GWASes) have identified numerous candidate genes that do not have clear roles in those processes previously identified (4), suggesting alternative mechanisms of pathogenesis. Hedgehog-interacting protein (HHIP) and patched 1 (PTCH1), both key modifiers of the hedgehog (Hh) pathway active during organ development, have been repeatedly implicated in multiple GWASes examining susceptibility to emphysema and lung function decline (5-11), but the functional relevance of this association remains unclear.

The Hh ligand functions as a morphogen that produces asymmetric activation domains during tissue development to generate diverse transcriptional outputs that translates into cellular diversity, and disruption of these spatial domains produces downstream patterning defects related to the loss of specific cellular position or function (12-14). Interestingly, Hh activation continues to be present in adult organs during normal homeostasis, particularly within the mesenchyme composed of cells such as fibroblasts,

smooth muscle, pericytes, and *etc.* that give rise to the connective tissues within the organs (15-19). In these organs, hedgehog is activated within a spatially restricted subset of the mesenchyme, where compartmental diversity is increasingly appreciated (20-22). Asymmetric Hh activation within the adult mesenchyme suggests that anatomical segregation of Hh-activation domains plays a role in the diversification of mesenchymal cell identity and maintenance of organ function, and disrupting the domain of Hh activation could lead to aberrant tissue remodeling.

The mammalian lung resembles an upside-down tree where the trachea enters the chest cavity and bifurcates into multiple generations of increasingly narrow conducting airway that ultimately terminates into highly sacculated alveoli where gas exchange takes place (23). Within both the human and murine lungs, the bronchoalveolar ductal junction (BADJ) marks the abrupt transition between the terminal airway and the alveoli where the epithelial composition differs markedly between the two compartments (24, 25). Putative stem/progenitor cells have been characterized at the BADJ(26, 27), including the bronchioalveolar stem cells (BASCs) with the capacity to differentiate into bronchiolar (SCGB1A1+) or alveolar (SFTPC+) epithelial stem/progenitor cells(28). Recent studies have suggested that the mesenchymal cells underlying these compartment-specific stem/progenitor cells have unique capacity to support the neighboring stem/progenitor cells, forming compartment-specific stem cell niches where epithelial-mesenchymal interactions dictate stem cell behavior(20, 22). We have previously shown that Hh is preferentially activated in the mesenchyme underlying the airway epithelium and less so in the alveoli, with the BADJ marking the transition point where the activation tapers

off(29). This suggests that Hh activation may play a role in differentiating the capacities of the stem cell niches of the proximal airway and distal alveoli to support their respective stem/progenitor cell populations through epithelial-mesenchymal feedback. For the rest of this study, we will refer to the airway structures of the mainstem bronchi to the BADJ as the proximal compartment and the alveolated lung distal to the BADJ as the distal compartment.

In this study, we developed a novel mouse tool to capture and genetically modify Hh-receptive mesenchyme in the adult lung, which is characterized by distinct subsets defined by unique transcriptomes and segregated by proximal-distal localization and levels of Hh activation. Disrupting the asymmetry of Hh through distal expansion of the activation domain results in aberrant mesenchymal identity that led to loss of alveolar gas exchange surface, regulated by a mesenchymal feedback loop to the alveolar stem cells. Single cell analysis of the human lung mesenchyme reveals a conserved segregation of proximal and distal mesenchymal transcriptomes characterized by asymmetric Hh activation. Our study sheds light on how asymmetric developmental pathway activation can serve to segregate cellular identity and maintain organ function in the adult, and illustrates how disruption of mesenchymal identity can disrupt the stem cell niche to induce loss of structural integrity as seen in chronic diseases such as emphysema.

Results

Asymmetric Hh activation in the adult lung mesenchyme

We first determined whether there is evidence for asymmetry of Hh activation within the adult lung, which is functionally and anatomically divided into the proximal conducting airway and the distal alveoli. We previously reported that Sonic hedgehog (*Shh*) ligand expression persists in the adult lung epithelium and activates the underlying mesenchyme (29). Here, we showed that *Shh* is highly expressed in airway proximal (SCGB1A1+) epithelium, with some expression in distal alveolar (SFTPC+) epithelium, by a combination of in situ hybridization and immunofluorescence staining (Supplemental Figure 1A). Consistently, when we examined transcriptional effectors of Hh activation, we found that *Gli1*, a transcriptional readout of highly active Hh signaling (30), was preferentially expressed in the mesenchyme surrounding the proximal conducting airway of the adult lung but largely absent from the distal alveoli (Figure 1A, top). In contrast, *Gli2*, a mediator of Shh activity whose expression does not depend on Hh activation (31), was expressed both around the proximal airway and in the distal alveoli of the adult lung (Figure 1A, bottom). Co-localization with *Pdgfra* demonstrated that *Gli2* was widely expressed in the distal alveolar mesenchymal fibroblasts that lack *Gli1* expression (Figure 1B).

To better isolate and study GLI2+ cells, we generated a *Gli2*$^{creERT2\text{-}tdT}$ mouse allele that allows us to isolate GLI2+ cells by endogenous *tdTomato* reporter expression, and activate Cre-inducible alleles within GLI2+ cells (Supplemental Figure 1B and C). Lineage analysis demonstrated that GLI2 only marks mesenchymal cells (Figure 1D and Supplemental Figure 1D). The expression of *Ptch1*, the receptor for SHH ligand, significantly overlaped with the expression of *Gli2* in both the proximal airway and distal

alveoli (Figure 1C), which suggests a broad domain of GLI2+ mesenchyme that is receptive to Hh signaling in both the proximal and distal compartment of the adult lung. Of note, the expression of *Ptch1* is also transcriptionally activated by the presence of Hh activation (32), and X-gal staining of the *Ptch1*$^{LacZ/+}$ reporter showed much higher intensity in the proximal compared to the distal mesenchyme (Supplemental Figure 1E), suggesting asymmetric activation of Hh within the broad GLI2+ mesenchymal domain.

To determine the degree of overlap between the GLI1+ and GLI2+ mesenchymal populations, we generated a *Gli1:Gli2* dual-color reporter (*Gli2*$^{creERT2\text{-}tdT}$*:Gli1*^{EGFP}). Flow cytometry analysis of *Gli2*$^{creERT2\text{-}tdT}$*:Gli1*^{EGFP} lungs digested into single cell suspension showed that the proximal GLI1+ mesenchyme constituted a subset entirely within a broader GLI2+ mesenchymal population in the adult lung (Figure 1D, right panel). Utilizing the *Gli1:Gli2* double reporter, we were able to separate and collect the proximal (GLI1+/GLI2+) from the distal (GLI1-/GLI2+) mesenchyme for RNA collection and downstream analysis. qPCR showed that the proximal mesenchyme was enriched in the expression of Hh target genes *Gli1*, *Ptch1*, *Ptch2* relative to the distal mesenchyme (Figure 1E). These data demonstrated a field of Hh-competent GLI2+ mesenchyme present in the adult lung, characterized by asymmetric Hh activation along the proximal (Hh^{HI})-distal (Hh^{LO}) axis (Figure 1F).

Asymmetric Hh activation promotes anatomical segregation of mesenchymal transcriptomes

To determine whether Hh activation segregates mesenchymal identity within the GLI2+ mesenchyme, we performed single cell RNA-sequencing (scRNA-seq) on sorted GLI2+ mesenchymal cells from the adult lung. We captured approximately 4,600 cells with a median of 2,246 genes detected per cell utilizing a droplet-based barcoding approach to capture single cells for transcript profiling (33). After filtering for sequencing quality and read depth (Supplemental Figure 2A and Methods), unsupervised graph-based clustering produced 4 distinct clusters (Figure 2A), with Cluster 1 and 2 comprising of 27 and 66 percent of the cells respectively while Clusters 3 and 4 combine to make up 7 percent of the total population. Differential expression analysis produced a list of signature genes for each subset (Supplemental Table 1). Immunofluorescence staining of cluster-specific signature genes confirmed that a small fraction of GLI2+ cells contribute to mesothelial (Cluster 3) and airway smooth muscle cells (Cluster 4) (Supplemental Figure 2B). Clusters 1 and 2 are associated based on common expression of fibroblast markers such as *Col1a1*, *Pdgfra*, and *Tcf21* (Supplemental Figure 2C), but they are segregated by markers that are anatomically-distinct. Validation of Cluster 1 markers demonstrates that they are predominantly expressed in the proximal fibroblasts surrounding the airway, whereas Cluster 2 markers are expressed in the fibroblasts in the distal alveoli (Supplemental Figure 2D). While both the proximal and distal mesenchymal fibroblasts have been shown to participate in matrix production and paracrine signaling with surrounding cells, Gene Ontology analysis of Cluster 1 and 2 signature genes showed that Cluster 1 (Proximal) was enriched in “Extracellular Matrix” genes (Fold enrichment: 5.33, p = 6.8e-6), while Cluster 2 (Distal) was enriched in “Cell-to-Cell Signaling” genes (Fold enrichment: 3.25 p = 4.4e-4, Figure 2B). To confirm that

the proximally located Cluster 1 was enriched for Hh-activated mesenchyme expressing *Gli1*, we performed flow cytometry analysis of signature genes expressed on the cell surface chosen from Cluster 1 and 2 in the *Gli1:Gli2* (*Gli2*$^{creERT2\text{-}tdt}$*:Gli1*^{EGFP}) dual-color reporter mouse lungs. Flow cytometry analysis demonstrated that Cluster 1 markers, *Ly6a* and *Ly6c1*, were enriched in the GLI1+ fraction of the GLI2+ mesenchyme (Figure 2C). Conversely, Cluster 2 marker, *Itga8*, wass enriched in the GLI1- fraction of the GLI2+ mesenchyme (Figure 2C). This suggests that the GLI2+ population is segregated into distinct mesenchymal subtypes along the proximal-distal axis of the lung characterized by asymmetric Hh activation.

Next, we tested to see if Hh is a determinant of proximal identity where it is preferentially activated, rather than just a marker. We over-expressed a constitutively active form of the Hh effector, *Smo* (*SmoM2*) (34), throughout the entire GLI2+ mesenchyme, expanding Hh activation into the distal mesenchyme (Figure 2D). To determine whether expansion of Hh activation promotes proximal vs. distal identity, we performed bulk RNA-seq of the sorted GLI2+ mesenchyme and performed gene set enrichment analysis of the genes upregulated and downregulated by Hh expansion with the proximal and distal mesenchymal fibroblast gene signature sets (top 100 genes) identified by scRNA-seq. The proximal signature genes were significantly enriched amongst genes up-regulated in the Hh-expanded samples versus control (CAMERA $p<0.0001$, $FDR<0.0001$, Figure 2E, Supplemental Figure 3A, and Supplemental Table 2). Conversely, distal signature genes were significantly enriched amongst genes down-regulated in the Hh-expanded samples (CAMERA $p<0.0001$, $FDR<0.0001$, Figure 2E, Supplemental Figure 3A, and

Supplemental Table 3). qPCR analysis of the ITGA8+/GLI2+ distal mesenchyme confirmed upregulation of proximal genes within the distal domain in Hh-expanded mutants vs. controls (Supplemental Figure 3B). These data showed that Hh functions as a "selector gene" (35) within a field of Hh-competent mesenchyme in the adult lung, maintaining diversification by asymmetrically promoting proximal while suppressing distal mesenchymal identity in a spatially restricted manner.

Distal expansion of Hh activation induces emphysema

As recent GWASes have repeatedly implicated modifiers of Hh signaling in COPD/emphysema susceptibility and severity (5, 6, 10), we examined the transcriptome profiles of COPD/emphysema patients in the largest study to date that correlated gene expression within epithelial brushings with clinical disease severity (36). As the study only sampled the epithelium, we examined the expression of Hh ligands, *SHH*, *IHH*, and *DHH*, that are expressed in the lung epithelium. Using a regression model that adjusts for gender, smoking status, age, and pack-years smoked, we found that *SHH* expression in the epithelium significantly correlates with disease severity as measured by FEV1 (Supplemental Figure 4A, $p=3.09 \times 10^{-8}$), the primary measure of lung function used to stratify COPD/emphysema (lower FEV1 = more severe disease). The expression of *IHH* and *DHH*, expressed in much lower abundance compared to *SHH*, are not significantly associated with lung function (Supplemental Figure 4A). Our transcript analysis of sorted epithelium in mouse and humans shows that *SHH* was the predominant Hh ligand expressed in the lung (Supplemental Figure 4B), which was elevated with increasing severity of COPD/emphysema. Next, we examined *Shh* expression in a well-established

murine model of emphysema utilizing cigarette exposure. Histological analysis of lungs exposed to 6 months of cigarette smoke demonstrated expansion of *Shh* expression by in situ in the distal alveoli compared to room air controls (Supplemental Figure 4C).

Increased expression of *SHH* in human COPD/emphysema and expansion of *Shh* expression in murine model of COPD/emphysema suggest that Hh over-activation can induce emphysema, so we investigated the effect of ectopic activation of Hh on the distal airspace morphology of the Hh-expanded and control animals. Inducible expansion of Hh activation within the GLI2+ mesenchyme induced over twenty percent enlargement of airspace compared to controls, as characterized by increase in mean linear intercept (chord) length and alveolar size, along with reduced density of alveoli in the distal lung that are hallmarks of emphysema (Figure 3A). Furthermore, the mutants also display a more simplified alveolar structure where secondary crests are absent from the enlarged alveoli that are characteristics of emphysema as well as alveolar developmental delay syndromes such as bronchopulmonary dysplasia (37) (Supplemental Figure 5A). In addition to histological analysis of the airspace morphology, we also developed a radiographic method to quantify the degree of emphysema based on X-ray attenuation on computed tomography (CT) in explanted whole lungs. Human emphysematous lungs demonstrate increase in percentage of low attenuation areas (%LAA) on CT due to destruction of alveolar structures resulting in large areas of air that appears as black space on CT (38). Similarly, we performed micro-CT of murine lungs of both control and Hh-expanded mutants followed by 3D volume rendering to quantify the percentage of low attenuation volume (LAV) as a ratio of the total lung volume (TLV). Hh-expanded

mutant lungs demonstrated significantly elevated LAV/TLV ratio compared to controls (Figure 3B), consistent with the histological findings of airspace enlargement.

To determine whether this phenotype is due to Hh activation in the proximal or distal mesenchyme, we utilized a transgenic *Pdgfra*^{creERT2} allele where lineage labeling only occurs in the distal mesenchyme at our operating tamoxifen dose while sparing the proximal mesenchyme (Supplemental Figure 5B). Activation of the *SmoM2* allele (*Pdgfra*^{creERT2}*:R26R*$^{YFP/SmoM2}$) within the distal mesenchyme phenocopied the airspace morphology changes seen in the Hh-expanded mutant using the *Gli2* allele, resulting in enlarged alveoli with reduced alveolar density (Figure 3D). In fact, the airspace enlargement phenotype seen with Hh expansion using the *Pdgfra*^{creERT2} driver was more severe compared to the *Gli2*$^{creERT2\text{-}tdT}$ driver, which was likely due to the difference in expression level of the genes driving the *creERT2* expression. In contrast, we can induce Hh activation only within the proximal mesenchyme while sparing the distal mesenchyme using the *Gli1*^{creERT2} (Supplemental Figure 5B), and *Gli1*^{SmoGOF} (*Gli1*^{creERT2}*:R26R*$^{YFP/SmoM2}$) mutants did not display significant distal airspace morphological changes compared to controls (Figure 3E). This showed that domain-specific activation of Hh in the distal mesenchyme induces airspace enlargement similar to emphysema, a lung disease linked to Hh signaling in multiple large-cohort GWASes.

Hh expansion disrupts the distal alveolar niche

While the prevailing notion of emphysema ascribes the loss of alveoli to excessive inflammation most commonly due to tobacco exposure (1), we did not observe evidence

of increased inflammatory cells in the lungs of the Hh-expanded mutants when we examined the leukocytes present in the bronchoalveolar lavage fluid (BALF) as well as the composition of immune cells in the digested lungs by flow cytometry (Figure 3C and Supplemental Figure 6A). We also did not observe an increase in the number of apoptotic cells as indicated by cleaved-caspase 3 staining in the lungs of controls and mutants (Supplemental Figure 6B). However, we did notice the loss of SFTPC+ type 2 pneumocytes, a putative resident stem cell in the distal alveoli(39), from the distal alveolar region of Hh-expanded mutants (Figure 4A). Distal expansion of Hh disrupted normal alveolar stem cell renewal, as Hh-expanded (*Gli2*^{SmoGOF}) mutants demonstrated significantly reduced fraction of SFTPC+ alveolar stem cells that incorporated BrdU compared to controls during normal homeostasis as well as injury with bleomycin (Figure 4B-D). This data showed that Hh activation in the distal mesenchyme could attenuate alveolar stem cell renewal in a non-cell autonomous manner, possibly altering mesenchymal feedback to the stem cells.

Amongst the genes identified in the distal mesenchymal fibroblast signature that was enriched in “Cell-to-Cell Signaling” was *Hgf*, a mesenchymal-derived mitogen implicated in stem cell renewal (19). We confirm that *Hgf* is expressed in distal alveolar mesenchyme by in situ (Figure 4E), and deficiency of HGF in the lung has been linked to emphysema (40, 41). Immunofluorescence staining of the lung shows that the HGF receptor, *Met*, is expressed almost exclusively in the SFTPC+ distal alveolar stem cells that are adjacent to Gli2+ distal mesenchyme in vivo (Figure 4F), suggesting that Hh

activation in the distal alveolar mesenchyme might regulate HGF activation of MET in the alveolar stem cells.

To determine the effect of Hh activation on the distal alveolar niche in vitro, we first generated a transgenic animal (*Ubc*^{creERT2}*:R26R*$^{SmoM2/+}$) where constitutively active SmoM2 could be induced in isolated lung mesenchymal cells in vitro utilizing a *creERT2* allele driven by a ubiquitously expressing promoter (42). Addition of 4-hydroxytamoxifen (4OHT) to the Hh-inducible lung mesenchymal fibroblasts activated *Gli1* expression while *Hgf* expression was downregulated (Figure 5A). We then co-cultured the Hh-inducible mesenchyme with isolated SFTPC+ distal alveolar stem cells, and mesenchymal Hh activation with 4OHT resulted in significantly reduced distal alveolar organoid growth compared to vehicles, which was rescued with escalating doses of recombinant HGF (Figure 5B). HGF interaction with the MET receptor induces MET autophosphorylation to activate the tyrosine kinase activity of the receptor(43). To determine whether Hh expansion in the distal alveolar mesenchyme affected MET activation in vivo, we quantified MET phosphorylation in the Hh-expanded lungs, and showed that ectopic Hh activation in the alveolar mesenchyme reduced the ratio of phosphorylated MET to total MET (Figure 5C).

Deletion of *Met* during lung development and maturation has previously been shown to disrupt normal alveolarization (44). To determine whether the HGF-MET axis plays a role in maintaining the distal alveolar airspace during adult homeostasis *in vivo*, we inducibly deleted *Met* from the SFTPC+ alveolar stem cells by generating a *Sftpc*^{creERT2}*:Met*$^{flox/flox}$

(*Sftpc*^{MetCKO}) mutant. Tamoxifen induction of the adult *Sftpc*^{MetCKO} mutant resulted in a similar enlargement of alveolar airspace and loss of alveolar density (Figure 5D) as previously seen in the Hh-expanded mutants utilizing both the *Gli2* and *Pdgfr*α *creERT2* alleles. These results showed that expansion of Hh activation disrupts distal mesenchymal feedback to the alveolar stem cells via HGF-MET signaling that maintains normal alveolar homeostasis, and contributes to emphysematous changes in the distal lung.

In addition HGF-MET signaling, recent studies have shown that Wnt ligands are enriched in the alveolar mesenchyme, which provides mitogenic cues to Wnt-receptive alveolar stem cells (45, 46). Here, we showed that activation of the Hh-inducible mesenchymal fibroblasts *in vitro* suppressed the expression of *Wnt1*, *Wnt2*, *Wnt3a* and *Wnt7b* (Supplemental Figure 7A), and the addition of Wnt-agonist, Chiron (CHIR), also partially rescued the defect in SFTPC+ distal alveolar stem cells proliferation resulting from Hh-activation in the mesenchyme (Supplemental Figure 7B). This suggests that Hh activation could suppress a broad program of mitogenic feedback to the epithelial stem cell compartment in the distal alveoli.

Hedgehog asymmetry and mesenchymal segregation is conserved in the human lung

To determine whether the human lung mesenchyme exhibit similar segregation of transcriptomes based on anatomical location, we performed scRNA-seq on the human lung mesenchyme. We isolated lung specimen from both the proximal portion enriched in

airways and distal portion enriched in alveoli separately. The lung fragments were then digested and FACSorted for mesenchymal cells based on negative expression of epithelial, hematopoietic, and endothelial markers (EPCAM-/CD45-/CD11b-/CD31-). Library preparation was performed separately for the proximal and distal-derived mesenchymal cells so that each subset has distinctive barcodes to determine anatomical origin (Figure 6A and Supplemental Figure 8A), and approximately 10,000 cells were captured from each specimen (Supplemental Figure 8B), which were then merged for analysis. Unsupervised clustering with hierarchical analysis of gene expression of the merged datasets reveals three distinct subsets of mesenchyme based on transcriptome identity (Figure 6B and C), with Clusters 1 and 2 (C1 and C2) demonstrating distinct segregation and enrichment of cells from the proximal and distal-derived fragments respectively (Figure 6A), and immunofluorescence staining confirms localization of cluster signature genes to the proximal airway or distal alveoli (Supplemental Figure 8C). Cluster 3 shared some gene expression patterns with both proximal and distal subsets with a smaller number of unique genes, and we labeled this cluster “intermediate” (Figure 6B and C). Applying the same pipeline to identify subset-specific signature genes (Supplemental Table 4), we found that the proximal and distal human lung mesenchymal subsets demonstrated significant overlap of homologous genes with their murine counterparts (human and murine proximal, odds ratio 8.2, p = 2.4e-12, human and murine distal, odds ratio 11.8, p = 2.2e-14, Figure 6D and E), while the human intermediate subset did not resemble either murine subset (Supplemental Figure 8D and E). Similar to the mouse lung, Gene Ontology analysis of the human lung mesenchymal signature genes also found enrichment in “Extracellular Matrix” (Fold enrichment: 6.24, p

= 1.2e-19) and “Cell Communication” (Fold enrichment: 1.6, p = 7.6e-9) genes in the proximal and distal subsets respectively, suggesting a segregation of mesenchymal function based on anatomical location that is conserved across species (Figure 6F). The intermediate mesenchymal subset, which was novel compared to the murine mesenchymal subsets, was enriched for genes involved in “Cholesterol metabolism” (Fold enrichment: 14.9, p = 1.7e-4, Supplemental Figure 8E), which suggests that it might function as putative lipofibroblasts that promote surfactant biosynthesis in the alveolar epithelium (47). Furthermore, we were able to separate the proximal and distal mesenchyme by FACSorting with antibodies against cell-surface markers (THY1 and ITGA8, markers of proximal and distal mesenchymal identity respectively in both mouse and human lungs) enriched in each subset (Supplemental Figure 8F). qPCR analysis of the sorted mesenchymal cells demonstrated that proximal (THY1+) mesenchyme was enriched in Hh target genes relative to the distal mesenchyme (ITGA8+) (Figure 6G), reflecting a similar asymmetry of Hh activation seen in the murine lung. This demonstrated that segregation of mesenchymal identity based on asymmetric Hh activation is a conserved organizational feature of the adult lung (Figure 6H).

Discussion

While region-specific diversity of the mesenchymal compartment is coming into focus in adult tissue, the mechanism to generate and maintain this diversity during normal homeostasis has not been defined. Our study demonstrated that adult organs continue to utilize a developmental morphogen whereby asymmetric Hh activation diversifies the mesenchyme into proximal and distal populations with distinct identity, which might

exhibit a level of plasticity modulated by the level of Hh activation (Figure 7A). Single cell transcriptome analysis identified distinct proximal and distal mesenchymal gene signatures that are in part maintained by asymmetric Hh activation in the mesenchyme in both the murine and human lung. In addition, we generated a model to disrupt the asymmetry of Hh activation in the lung mesenchyme by expanding the domain of Hh activation into the distal compartment, and utilized both single cell and bulk population RNA sequencing to demonstrate the disruption of distal mesenchymal identity, leading to loss of tissue integrity in the adult lung. While mesenchymal plasticity in the context of transdifferentiation between specific cell types (e.g. differentiation of lipofibroblast to myofibroblasts) during fibrotic injury have been recently described(48, 49), our study suggests that mesenchymal plasticity between region-specific subsets (e.g. distal to proximal mesenchyme and vice versa) may play a role in the tissue response and outcomes to injury repair.

Beyond its role of providing the structural scaffold of adult organs, the mesenchyme has been recognized as a vital component of the stem cell niche through reciprocal interactions with epithelial stem cells. We demonstrate that the distal mesenchyme is enriched in paracrine factors known to be important in stem cell maintenance and renewal. Recent work has shown that the presence of GLI2 in the mesenchyme is required for the expression of mammary epithelial stem cell niche signals that regulates ductal morphogenesis and maintenance (50), suggesting that GLI2 is a marker of specialized mesenchyme to support the stem cell compartment. In this study, we generated a new tool to isolate and dissect the GLI2+ mesenchyme, demonstrating that

GLI2+ mesenchyme participated in feedback to alveolar stem cells. Furthermore, we showed that the proper niche function is mediated by the asymmetric Hh activation, as expansion of Hh activation into the distal mesenchyme reduced its capacity to support the alveolar stem cells in the distal compartment of the lung, resulting in a loss of alveoli that resembles emphysema.

Multiple large-cohort genome-wide association studies have identified Hh signaling components, *HHIP* and *PTCH1*, as genetic determinants of emphysema and lung function respectively in humans (5, 7), but the mechanism underlying this association remains unclear. Both HHIP and PTCH1 negatively regulate the Hh pathway (51, 52), and enhancer analysis has shown that the polymorphisms of HHIP that confers susceptibility to emphysema are loss-of-function (53), implying a de-repressed Hh pathway in those with genetic susceptibility to emphysema. This study showed that disruption of the Hh gradient through ectopic activation in the distal mesenchyme induces emphysematous changes in the murine lung, in part by disrupting the mesenchymal feedback of HGF to the distal epithelial stem cells in the alveoli (Figure 7B).

A limitation of our study is that we have not established a direct link between loss of *HHIP,* the Hh signaling component most commonly associated with human emphysema*,* with the gain-of-function Hh phenotype that we have utilized to induce an emphysematous phenotype in mouse models. Future studies addressing the role of HHIP in modulating Hh signaling in the adult lung are necessary to address the potential

mechanistic role of Hh in human emphysema. Another caveat of our study is that we could not find alterations in inflammation or apoptosis in our murine model of emphysema, which does not exactly recapitulate the human disease. Finally, although we provide evidence that the SHH ligand is elevated in COPD/emphysema patients along with novel single cell transcriptome studies showing differential expression of Hh targets in human fibroblast subsets, further studies in human emphysema tissues are required to determine whether region-specific identities are altered in the disease. While we acknowledge that the pathogenesis of human emphysema is multifactorial, we do believe that our study combined with the GWASes offer a novel paradigm where ectopic Hh activation can disrupt mesenchymal feedback to the stem cell compartment to cause alveolar loss to contribute to the emphysema phenotype.

Methods

Animal studies

Generation and genotyping of the *Gli2*^{lacz}, *Gli1*^{lacz}, *Gli1*^{EGFP}, *Gli1*^{creERT2}, *Scgb1a1*^{creERT2}, Ptch1lacz, *Pdgfra*^{creERT}, *Pdgfra*^{GFP}*;Ubc*^{creERT2}, *c-Met*$^{flox/flox}$, *R26R*^{SmoM2}, *R26R*^{EYFP} lines have been previously described and obtained from JAX. *Gli1*^{EGFP} strain was obtained through GENSAT(54). *SFTPC*^{creERT2} was generated as previously describe (55). To generate the *Gli2*$^{creERT2\text{-}tdT}$ mouse, a *CreERT2-2A-tdTomato* expression cassette was inserted into the ATG site in exon2 of the *Gli2* locus (Supplemental Figure 1B). Targeting vector construction, ES cell selection and injection were performed by Ingenious Targeting Laboratory (Ronkonkoma, NY, USA). The presence of the *Gli2-Cre-ERT2-2A-tdTomato* allele was determined by genomic DNA PCR with a wild-type band of 230 bp and a mutant band of 500 bp (Genotyping primer for *Gli2*$^{creERT2\text{-}tdT}$ Common Forward: CCTGGGGTCAGAAGACTGAG, WT Rev: CTGCTGTCCTCCAAGAGACC, Mut Rev: CCAGTGAAACAGCATTGCTGT). Animals between the ages of 8-12 weeks old were used for the experiments and littermates were used as controls with balance of gender between groups. Unless otherwise indicated all mice were maintained on a mixed background. Tamoxifen (Sigma) was dissolved in corn oil and administered intraperitoneally at 200mg/kg per day x 3 days for lineage tracing studies, with the exception of *Gli2*$^{creERT2\text{-}tdT}$, which was given at 200mg/kg per day x 5 days. For injury experiments, bleomycin (Hospira) was dissolved in PBS and injected *i.p.* at 50U/kg animal for twice a week x 4 weeks. For Brdu tracking experiment, mice were supplied water with 0.5 mg/ml Brdu (Sigma) and 1% sucrose continuously for 4 weeks. All animals were housed and treated in accordance with the IACUC protocol approved at

the University of California, San Francisco. For cigarette smoke exposure, 8 weeks old C57BL/6J mice were exposed to room air or the smoke from nonfiltered research cigarettes (2R4; University of Kentucky, Lexington, KY) as previously described (56). During the first week, mice received half a cigarette twice a day to allow for acclimation, and then two cigarettes per day (one cigarette per session, two sessions per day) for up to 6 months.

Human lung collection

Human lungs were received from brain-dead donors from the Northern California Transplant Donor Network. Screening criteria for selection of healthy lung for specimen collection was previously described (57).

Murine cell culture and organoid assay

For *Ubc*^{creERT2}*:R26R*^{SmoM2} mesenchymal cells, lung was digested as above and then cells were cultured on gelatin-treated tissue culture plates with DMEM-F12 plus 10% FBS. Media was refreshed every other day and primary lung mesenchymal cells were maintained for no more than three passages. The *Ubc*^{creERT2}*:R26R*^{SmoM2} mesenchymal cells were pretreated with vehicle or 1ug/ml 4-OH-tamoxifen for 72 hrs before co-culturing with epithelium. For organoid assay, GFP+ alveolar epithelium were FACS sorted from tamoxifen induced *SPC*^{creERT}*:R26R*^{mTmG} lungs, and co-cultured with *Ubc*^{creERT2}*:R26R*^{SmoM2} mesenchymal cells ($5x10^3$ epithelial cells : $3x10^4$ mesenchymal cells/well) in a modified small airway epithelial cell growth medium (SAGM) diluted 1:1 in growth factor reduced Matrigel (Corning). The modified SAECM is comprised of SAGM

(PromoCell) with selected components from SAGM bullet kit (PromoCell) including 5 μg/ml insulin, 10 μg/ml transferrin, 0.004 ml/ml bovine pituitary extract, 0.1 ng/ml retinoic acid and 10 ng/mL EGF. Additional components include 0.1 ug/mL cholera toxin (Sigma) and 5% FBS (Life Technologies). Cell suspension-Matrigel mixture was placed in a transwell and incubated in growth media with 10 μM ROCK inhibitor (Sigma) in a 24 well plate for 48 hrs, after which the media was replenished every 48 hrs (lacking ROCK inhibitor). Recombinant HGF (R&D Systems) was added at 20 ng/ml and 100 ng/ml, CHIR (DMSO was used as control) was added at 20 nM after 48 hrs and replenished every 2-3 days. Colonies are assayed after 14 days. Each experimental condition was performed in triplicates and counted blinded to the experimental condition. Colony forming efficiency = (number of GFP+ colonies/number GFP+ epithelial cells cultured per well). Areas of individual colonies are assayed on Fiji and over 140 colonies are randomly sized per experimental condition.

Single cell capture and sequencing

Gli2+ murine cells and human lung mesenchymal cells (EPCAM-/CD45-/CD31-/CD11b-) were sorted as described above and resuspended in 50 μL PBS with 0.04% BSA at 1,000 cells/μL, and loaded onto a single lane into the Chromium™ Controller to produce gel bead-in emulsions (GEMs). GEMs underwent reverse transcription for RNA barcoding and cDNA amplification, with the library prepped with the Chromium Single Cell 3' Reagent Version 2 kit. Sample was sequenced on the HiSeq2500 (Illumina) in Rapid Run Mode.

RNAscope in situ hybridization

Mouse *Shh*, *Hgf*, *Fbln2*, *Thy1*, and *Npnt* probes for RNA in situ detection were purchased from Advanced Cell Diagnotics. Paraffin-embedded lung sections were processed for RNA in situ detection using the RNAscope Multiplex Fluorescent Reagent Kit v2 (Advanced Cell Diagnotics) according to the manufacturer's instructions.

Expression overlay image analysis

Sections included in cell count analysis were acquired using confocal microscopy. At least three animals per genotype were used, at least 5 randomly selected sections were chosen for each animal. Cell counts were performed on Fiji using the "Cell Counter" plug-in and performer was blinded to the specimen genotype and condition. Results were averaged between each specimen and standard deviations were calculated per genotype. One tailed Student's t-test was used to determine the p value.

Mean linear intercept (MLI), airspace size and alveolar density analysis

For alveolar morphometric analysis, mouse lungs were processed according to the above protocol for paraffin embedded samples, with the exception of inflation with 4% PFA with a constant pressure of 25 cm H_2O. The paraffin-embedded lung sections were stained by hematoxylin and eosin (H&E) for analyzing alveolar morphology metric. At least 5 randomly selected sections from each genotype were selected for analysis. The MLI was calculated as the linear sum of the lengths of all lines randomly drawn across the images, divided by the number of intersections between alveolar walls. A minimum of 1000 intercepts from 60 lines drawn across the lung in a randomized fashion were

obtained for each lung, and the analysis was carried out on Fiji with the “Cell Counter” plug-in. The airspace size was measured on Fiji using the “Analyze Particles” tool. Image was first converted to 8 Bit and inverted, and “Analyze Particle” function used with set minimum of 50 um^2 and max of infinity to identify and quantify alveoli in the image. The average airspace size for each lung was quantified with dividing the total airspace by the number of alveoli. At least 3,500 alveoli were measured for each lung. The alveolar density was the reciprocal of the airspace size. The airspace of airway and pulmonary vessels was excluded. Statistical analysis was done using the one tailed Student’s t-test. Data are presented as means ± SEM.

Contrast-enhanced microCT imaging of lung airspace

Lung specimens were harvested and fixed in 4% PFA at 4 ºC for 24 hours. Specimens were then washed four times in PBS for 30 minutes each. Lungs were stained in a 25% Lugol’s iodine solution at 4°C for 48 hours. Specimens were then embedded in a scanning medium of 3% agarose. Following agarose embedding, lung specimens were scanned on a Scanco Medical µCT 50 high-resolution specimen scanner. X-ray energy was set at 45 kVp and 88 µA. Specimens were scanned at a resolution of 10-µm voxel size and using an integration time of 500 ms. Quantitative analyses were performed using Scanco µCT Evaluation Program. The region of interest was manually delineated slice-by-slice to include the entire lung volume which we call total lung volume (TLV). An upper threshold of 160 grayscale units, out of 1000, was applied to segment airspace and exclude tissue. A Gaussian filter with sigma of 0.8 and support of 1 was applied to

remove background noise and the airspace volume which we call low attenuation volume (LAV) is then quantified and reported as a ratio of LAV/TLV for each specimen.

Single-cell RNA-Seq analysis

To build transcript profiles of individual cells the CellRanger v1.1.0 software with default settings was used for de-multiplexing, aligning reads with STAR software to mouse genome GRCm38 and Hg19 for human, and counting unique molecular identifiers (UMIs). We used the Seurat v2.0 R package along with a gene-barcode matrix provided by CellRanger for downstream analysis (62). In total, we filtered the data in 2 different steps. We first filter the dataset by only accepting cells that contained about 200 genes/cell and genes that were expressed in at minimum of 3 cells. The UMI were log-normalized and we to the identified genes with high expression and those are variable we used the mean variance relationship method. Our second filtered was set to accept cells with up to 4500 UMIs and a percent.mito cut off $2X10^{-5}$ for mouse data and 5000 UMIs with percent.mito cut off 0.1 for human data. Using regress out function, we took out cells that contain high mitochondrial genes. Next we used principle component analysis (PCA) to identify components that can be found within our dataset for unsupervised clustering. We used the JackStrawPlot function in the Seurat function to create Scree plots were and compare p-value (significance) for each PC. We selected 10 different PCA's for un supervised clustering of both datasets. Clustering results were visualize using the t-distributed stochastic neighbor embedding (TSNE) algorithm in the Seurat package. For the mouse data 7 clusters were identified, but 2 clusters were not analyzed because they contained less than 10 cells, and 1 cluster was suppressed

because it contained >10% mitochondrial genes in the top 50 genes in adjusted p value, leaving 4 main clusters. In the human data set we found 4 clusters that encompassed the mesenchyme which was divided intro proximal, intermediate and distal clusters. Differentially expressed genes between clusters were identified using Cell Ranger via sSeq method which employs a negative binomial exact test. The algorithm runs for each cluster against the rest of the clusters through a fast asymptotic beta test used in edgeR. Cell Ranger computes relative library size as the total UMI counts for each cell divided by the mean UMI counts per cell as a way to normalize by the per cell library size, which is a parameter incorporated in calculations of differentially expressed genes. Dotpots were created using the Seurat DotPlot function to visualize the percent of cells expressing a gene and the average expression level between our clusters. For cluster visualization and individual gene visualization on all clusters we used the TSNE function. Gene ontology enrichment analysis was performed using the PANTHER Overrepresentation test (www.geneontology.org) and entering the top 250 over-expressed genes in each cluster. Odds ratio and p value of overlap between mouse and human mesenchymal subsets were calculated using Fisher's Exact Test for enrichment using a base value of 21,000 genes in the mouse and human genome respectively.

Bulk RNA-seq data analysis

Sequencing was done using Sanger/Illumina 1.9 and we got an average of 45 million reads per sample with a total of 4 biological replicates per condition. Quality control of reads was conducted by using FASTQC. Ligation adaptors were removed using the Cutadapt and Sickle. Sequencing reads were aligned using HISAT and assembled with

Stringtie software to the reference genome *Mus musculus* UCSC version mm10. All gene counts of the biological replicates were concatenated while running DEseq for differential gene expression.

CAMERA gene set enrichment analysis

We used CAMERA (competitive gene set test accounting for inter-gene correlation) to compare the single cell sequencing datasets with the whole tissue dataset (63). Camera determines whether a group of genes ("gene set") is significantly over-represented ("enriched") at extremes of a ranked list, in which case the gene set is considered correlated with the phenotype. This is done using a rank-based test, an extension of the Wilcoxon Mann Whitney that adjusts for inter-gene correlation amongst the test set. The analysis was carried out using the limma package in the R statistical environment. Raw gene counts from the whole tissue experiment were first filtered to include only those genes indexed in the HGNC database and with Ensembl gene biotype of "protein_coding". Gene with low or zero counts were removed by filtering out genes with less than 50 total read counts across samples. Gene counts were then normalized using the limma voom function and this dataset was used as the test set in the CAMERA analysis. Four gene sets from the single cell sequencing experiments were generated to analyze against this test set in the CAMERA analysis. These four gene sets were derived from the top 100 genes significantly upregulated (fold-change>1.5, FDR<0.05) in association with (1) the proximal phenotype, (2) the distal phenotype.

Human lung epithelial brushing transcriptome analysis

Bronchial epithelial brushings obtained from 6th-8th generation bronchi of former and current smokers with (n=85) and without COPD (n=152) were previously profiled by Affymetrix HG 1.0 ST Arrays (Santa Clara, CA) (36). Spirometry was done in all participants. Raw microarray files may be downloaded from the Gene Expression Omnibus (GEO, accession: GSE37147). Inclusion/exclusion criteria were previously published. The microarray dataset underwent quantile normalization and probe summarization using the RMA algorithm (affy package, Bioconductor, R). Entrez gene custom chip definition files available at http://brainarray.mbni.med.umich.edu were used for annotation. Batch effect was minimized using Combat. Regression analyses were performed using the limma package in R, between log2 gene expression forced expiratory volume in one second (FEV1). Analyses were done before and after adjustment for age, gender, smoking status, and pack-years.

Data access

The accession number for the sequencing data reported in this paper are NCBI GEO: GSE 102592 for both the single-cell RNAseq and bulk RNAseq datasets.

Statistics

Statistical analysis was carried out using GraphPad Prism software. One-tailed Student's t tests were used to generate P values. One-way analysis of variance (ANOVA) was used to determine whether there were statistical differences among three groups followed by Fisher's least significant difference (LSD) test for pairwise comparisons if the

overall test was statistically significant. A P value less than 0.05 was considered significant.

Study approval

All mice were maintained under specific pathogen-free conditions at UCSF according to IACUC protocol AN111302. The human lung specimens are derived from brain-dead donors and de-identified from the deceased donor, therefore not applicable to human subjects research under HHS regulations.

Author contributions

C.W. and T.P. conceived the experiments. C.W., R.M., M.C., P.S. and A.B. performed the experiments. C.W. and R.M. performed flow cytometry and histological analysis. N.R.M. and L.B., performed analysis of single-cell RNAseq dataset. N.R.M. and S.C. performed analysis of bulk RNAseq dataset. M.M. and D.J. procured human lung specimen. A.L. performed imaging acquisition and analysis of lung microCT. J.S., Y.Y., and H.C. provided expertise and feedback. T.P. and C.W. wrote the manuscript.

Acknowledgements

We thank Christopher Law, Zimu Deng, Julia Jackson, Andrew Vaughan, Ian Driver, and David Frank for providing technical assistance; Ophir Klein for sharing in situ hybridization resources; Ed Morrisey for providing the CreERT2-2A-tdTomato targeting cassette; Ari Molofsky for flow cytometry resources; Chris Gralapp for assistance with model illustration; Mark Looney Dean Sheppard, Ophir Klein, Prescott Woodruff, John

Fahy, and Rushika Perera for critical review of manuscript; the Parnassus Flow Cytometry Core for assistance with cell sorting for bulk and single cell RNA analysis; Eunice Wan and the Institute for Human Genetics Core for processing of single cell RNA samples and high-throughput sequencing. GEO accession number for raw RNA sequencing data is listed in Materials and Methods. T.P. is a NIH New Innovator and this work was supported by NIH grants DP2AG056034 and K08HL121146, and Marcus Precision Medicine and Pulmonary Hypertension Association award to T.P. Access to flow cyotmeters supported by DRC Center Grant NIH P30 KD063720 and NIH S10 1S10OD021822-01.

References

1. Tuder RM, Yoshida T, Arap W, Pasqualini R, and Petrache I. State of the art. Cellular and molecular mechanisms of alveolar destruction in emphysema: an evolutionary perspective. *Proc Am Thorac Soc.* 2006;3(6):503-10.
2. Wan ES, and Silverman EK. Genetics of COPD and emphysema. *Chest.* 2009;136(3):859-66.
3. Tuder RM, and Petrache I. Pathogenesis of chronic obstructive pulmonary disease. *J Clin Invest.* 2012;122(8):2749-55.
4. Berndt A, Leme AS, and Shapiro SD. Emerging genetics of COPD. *EMBO Mol Med.* 2012;4(11):1144-55.
5. Pillai SG, Kong X, Edwards LD, Cho MH, Anderson WH, Coxson HO, Lomas DA, Silverman EK, Eclipse, and Investigators I. Loci identified by genome-wide association studies influence different disease-related phenotypes in chronic obstructive pulmonary disease. *Am J Respir Crit Care Med.* 2010;182(12):1498-505.
6. Castaldi PJ, Cho MH, San Jose Estepar R, McDonald ML, Laird N, Beaty TH, Washko G, Crapo JD, Silverman EK, and Investigators CO. Genome-wide association identifies regulatory Loci associated with distinct local histogram emphysema patterns. *Am J Respir Crit Care Med.* 2014;190(4):399-409.
7. Hancock DB, Eijgelsheim M, Wilk JB, Gharib SA, Loehr LR, Marciante KD, Franceschini N, van Durme YM, Chen TH, Barr RG, et al. Meta-analyses of genome-wide association studies identify multiple loci associated with pulmonary function. *Nat Genet.* 2010;42(1):45-52.
8. Li X, Howard TD, Moore WC, Ampleford EJ, Li H, Busse WW, Calhoun WJ, Castro M, Chung KF, Erzurum SC, et al. Importance of hedgehog interacting protein and other lung function genes in asthma. *J Allergy Clin Immunol.* 2011;127(6):1457-65.
9. Castaldi PJ, Cho MH, Zhou X, Qiu W, McGeachie M, Celli B, Bakke P, Gulsvik A, Lomas DA, Crapo JD, et al. Genetic control of gene expression at novel and established chronic obstructive pulmonary disease loci. *Hum Mol Genet.* 2015;24(4):1200-10.
10. Pillai SG, Ge D, Zhu G, Kong X, Shianna KV, Need AC, Feng S, Hersh CP, Bakke P, Gulsvik A, et al. A genome-wide association study in chronic obstructive pulmonary disease (COPD): identification of two major susceptibility loci. *PLoS Genet.* 2009;5(3):e1000421.
11. Loth DW, Soler Artigas M, Gharib SA, Wain LV, Franceschini N, Koch B, Pottinger TD, Smith AV, Duan Q, Oldmeadow C, et al. Genome-wide association analysis identifies six new loci associated with forced vital capacity. *Nat Genet.* 2014;46(7):669-77.
12. Gurdon JB, and Bourillot PY. Morphogen gradient interpretation. *Nature.* 2001;413(6858):797-803.
13. Briscoe J, and Small S. Morphogen rules: design principles of gradient-mediated embryo patterning. *Development.* 2015;142(23):3996-4009.
14. Wassef M, and Joyner AL. Early mesencephalon/metencephalon patterning and development of the cerebellum. *Perspect Dev Neurobiol.* 1997;5(1):3-16.

15. Fabian SL, Penchev RR, St-Jacques B, Rao AN, Sipila P, West KA, McMahon AP, and Humphreys BD. Hedgehog-Gli pathway activation during kidney fibrosis. *Am J Pathol.* 2012;180(4):1441-53.
16. Liu L, Kugler MC, Loomis CA, Samdani R, Zhao Z, Chen GJ, Brandt JP, Brownell I, Joyner AL, Rom WN, et al. Hedgehog signaling in neonatal and adult lung. *Am J Respir Cell Mol Biol.* 2013;48(6):703-10.
17. Peng YC, Levine CM, Zahid S, Wilson EL, and Joyner AL. Sonic hedgehog signals to multiple prostate stromalmesenchymal stem cells that replenish distinct stromalmesenchymal subtypes during regeneration. *Proc Natl Acad Sci U S A.* 2013;110(51):20611-6.
18. Shin K, Lee J, Guo N, Kim J, Lim A, Qu L, Mysorekar IU, and Beachy PA. Hedgehog/Wnt feedback supports regenerative proliferation of epithelial stem cells in bladder. *Nature.* 2011;472(7341):110-4.
19. Lim A, Shin K, Zhao C, Kawano S, and Beachy PA. Spatially restricted Hedgehog signalling regulates HGF-induced branching of the adult prostate. *Nat Cell Biol.* 2014;16(12):1135-45.
20. Zepp JA, Zacharias WJ, Frank DB, Cavanaugh CA, Zhou S, Morley MP, and Morrisey EE. Distinct Mesenchymal Lineages and Niches Promote Epithelial Self-Renewal and Myofibrogenesis in the Lung. *Cell.* 2017;170(6):1134-48 e10.
21. Yang H, Adam RC, Ge Y, Hua ZL, and Fuchs E. Epithelial-Mesenchymal Micro-niches Govern Stem Cell Lineage Choices. *Cell.* 2017;169(3):483-96 e13.
22. Lee JH, Tammela T, Hofree M, Choi J, Marjanovic ND, Han S, Canner D, Wu K, Paschini M, Bhang DH, et al. Anatomically and Functionally Distinct Lung Mesenchymal Populations Marked by Lgr5 and Lgr6. *Cell.* 2017;170(6):1149-63 e12.
23. Robinson RJ, Russo J, and Doolittle RL. 3D airway reconstruction using visible human data set and human casts with comparison to morphometric data. *Anat Rec (Hoboken).* 2009;292(7):1028-44.
24. Thiesse J, Namati E, Sieren JC, Smith AR, Reinhardt JM, Hoffman EA, and McLennan G. Lung structure phenotype variation in inbred mouse strains revealed through in vivo micro-CT imaging. *J Appl Physiol (1985).* 2010;109(6):1960-8.
25. Miller FJ, Mercer RR, and Crapo JD. Lower Respiratory Tract Structure of Laboratory Animals and Humans: Dosimetry Implications. *Aerosol Science and Technology.* 1993;18(3):257-71.
26. Hong KU, Reynolds SD, Giangreco A, Hurley CM, and Stripp BR. Clara cell secretory protein-expressing cells of the airway neuroepithelial body microenvironment include a label-retaining subset and are critical for epithelial renewal after progenitor cell depletion. *Am J Respir Cell Mol Biol.* 2001;24(6):671-81.
27. Giangreco A, Reynolds SD, and Stripp BR. Terminal bronchioles harbor a unique airway stem cell population that localizes to the bronchoalveolar duct junction. *Am J Pathol.* 2002;161(1):173-82.
28. Kim CF, Jackson EL, Woolfenden AE, Lawrence S, Babar I, Vogel S, Crowley D, Bronson RT, and Jacks T. Identification of bronchioalveolar stem cells in normal lung and lung cancer. *Cell.* 2005;121(6):823-35.

29. Peng T, Frank DB, Kadzik RS, Morley MP, Rathi KS, Wang T, Zhou S, Cheng L, Lu MM, and Morrisey EE. Hedgehog actively maintains adult lung quiescence and regulates repair and regeneration. *Nature.* 2015;526(7574):578-82.
30. Ahn S, and Joyner AL. In vivo analysis of quiescent adult neural stem cells responding to Sonic hedgehog. *Nature.* 2005;437(7060):894-7.
31. Bai CB, Auerbach W, Lee JS, Stephen D, and Joyner AL. Gli2, but not Gli1, is required for initial Shh signaling and ectopic activation of the Shh pathway. *Development.* 2002;129(20):4753-61.
32. Agren M, Kogerman P, Kleman MI, Wessling M, and Toftgard R. Expression of the PTCH1 tumor suppressor gene is regulated by alternative promoters and a single functional Gli-binding site. *Gene.* 2004;330(101-14.
33. Macosko EZ, Basu A, Satija R, Nemesh J, Shekhar K, Goldman M, Tirosh I, Bialas AR, Kamitaki N, Martersteck EM, et al. Highly Parallel Genome-wide Expression Profiling of Individual Cells Using Nanoliter Droplets. *Cell.* 2015;161(5):1202-14.
34. Jeong J, Mao J, Tenzen T, Kottmann AH, and McMahon AP. Hedgehog signaling in the neural crest cells regulates the patterning and growth of facial primordia. *Genes Dev.* 2004;18(8):937-51.
35. Lawrence PA, and Struhl G. Morphogens, compartments, and pattern: lessons from drosophila? *Cell.* 1996;85(7):951-61.
36. Steiling K, van den Berge M, Hijazi K, Florido R, Campbell J, Liu G, Xiao J, Zhang X, Duclos G, Drizik E, et al. A dynamic bronchial airway gene expression signature of chronic obstructive pulmonary disease and lung function impairment. *Am J Respir Crit Care Med.* 2013;187(9):933-42.
37. Bourbon JR, Boucherat O, Boczkowski J, Crestani B, and Delacourt C. Bronchopulmonary dysplasia and emphysema: in search of common therapeutic targets. *Trends Mol Med.* 2009;15(4):169-79.
38. Wang Z, Gu S, Leader JK, Kundu S, Tedrow JR, Sciurba FC, Gur D, Siegfried JM, and Pu J. Optimal threshold in CT quantification of emphysema. *Eur Radiol.* 2013;23(4):975-84.
39. Barkauskas CE, Cronce MJ, Rackley CR, Bowie EJ, Keene DR, Stripp BR, Randell SH, Noble PW, and Hogan BL. Type 2 alveolar cells are stem cells in adult lung. *J Clin Invest.* 2013;123(7):3025-36.
40. Plantier L, Marchand-Adam S, Marchal-Somme J, Leseche G, Fournier M, Dehoux M, Aubier M, and Crestani B. Defect of hepatocyte growth factor production by fibroblasts in human pulmonary emphysema. *Am J Physiol Lung Cell Mol Physiol.* 2005;288(4):L641-7.
41. Kennelly H, Mahon BP, and English K. Human mesenchymal stromalmesenchymal cells exert HGF dependent cytoprotective effects in a human relevant pre-clinical model of COPD. *Sci Rep.* 2016;6(38207.
42. Ruzankina Y, Pinzon-Guzman C, Asare A, Ong T, Pontano L, Cotsarelis G, Zediak VP, Velez M, Bhandoola A, and Brown EJ. Deletion of the developmentally essential gene ATR in adult mice leads to age-related phenotypes and stem cell loss. *Cell Stem Cell.* 2007;1(1):113-26.
43. Naldini L, Vigna E, Narsimhan RP, Gaudino G, Zarnegar R, Michalopoulos GK, and Comoglio PM. Hepatocyte growth factor (HGF) stimulates the tyrosine kinase

activity of the receptor encoded by the proto-oncogene c-MET. *Oncogene.* 1991;6(4):501-4.
44. Calvi C, Podowski M, Lopez-Mercado A, Metzger S, Misono K, Malinina A, Dikeman D, Poonyagariyon H, Ynalvez L, Derakhshandeh R, et al. Hepatocyte growth factor, a determinant of airspace homeostasis in the murine lung. *PLoS Genet.* 2013;9(2):e1003228.
45. Nabhan AN, Brownfield DG, Harbury PB, Krasnow MA, and Desai TJ. Single-cell Wnt signaling niches maintain stemness of alveolar type 2 cells. *Science.* 2018;359(6380):1118-23.
46. Zacharias WJ, Frank DB, Zepp JA, Morley MP, Alkhaleel FA, Kong J, Zhou S, Cantu E, and Morrisey EE. Regeneration of the lung alveolus by an evolutionarily conserved epithelial progenitor. *Nature.* 2018;555(7695):251-5.
47. Torday J, and Rehan V. Neutral lipid trafficking regulates alveolar type II cell surfactant phospholipid and surfactant protein expression. *Exp Lung Res.* 2011;37(6):376-86.
48. Plikus MV, Guerrero-Juarez CF, Ito M, Li YR, Dedhia PH, Zheng Y, Shao M, Gay DL, Ramos R, Hsi TC, et al. Regeneration of fat cells from myofibroblasts during wound healing. *Science.* 2017;355(6326):748-52.
49. El Agha E, Moiseenko A, Kheirollahi V, De Langhe S, Crnkovic S, Kwapiszewska G, Szibor M, Kosanovic D, Schwind F, Schermuly RT, et al. Two-Way Conversion between Lipogenic and Myogenic Fibroblastic Phenotypes Marks the Progression and Resolution of Lung Fibrosis. *Cell Stem Cell.* 2017;20(2):261-73 e3.
50. Zhao C, Cai S, Shin K, Lim A, Kalisky T, Lu WJ, Clarke MF, and Beachy PA. StromalMesenchymal Gli2 activity coordinates a niche signaling program for mammary epithelial stem cells. *Science.* 2017;356(6335).
51. Chuang PT, and McMahon AP. Vertebrate Hedgehog signalling modulated by induction of a Hedgehog-binding protein. *Nature.* 1999;397(6720):617-21.
52. Chen Y, and Struhl G. Dual roles for patched in sequestering and transducing Hedgehog. *Cell.* 1996;87(3):553-63.
53. Zhou X, Baron RM, Hardin M, Cho MH, Zielinski J, Hawrylkiewicz I, Sliwinski P, Hersh CP, Mancini JD, Lu K, et al. Identification of a chronic obstructive pulmonary disease genetic determinant that regulates HHIP. *Hum Mol Genet.* 2012;21(6):1325-35.
54. Gong S, Zheng C, Doughty ML, Losos K, Didkovsky N, Schambra UB, Nowak NJ, Joyner A, Leblanc G, Hatten ME, et al. A gene expression atlas of the central nervous system based on bacterial artificial chromosomes. *Nature.* 2003;425(6961):917-25.
55. Chapman HA, Li X, Alexander JP, Brumwell A, Lorizio W, Tan K, Sonnenberg A, Wei Y, and Vu TH. Integrin alpha6beta4 identifies an adult distal lung epithelial population with regenerative potential in mice. *J Clin Invest.* 2011;121(7):2855-62.
56. Zhang X, Shan P, Homer R, Zhang Y, Petrache I, Mannam P, and Lee PJ. Cathepsin E promotes pulmonary emphysema via mitochondrial fission. *Am J Pathol.* 2014;184(10):2730-41.
57. Lee JW, Fang X, Gupta N, Serikov V, and Matthay MA. Allogeneic human mesenchymal stem cells for treatment of E. coli endotoxin-induced acute lung

injury in the ex vivo perfused human lung. *Proc Natl Acad Sci U S A.* 2009;106(38):16357-62.
58. Peng T, Tian Y, Boogerd CJ, Lu MM, Kadzik RS, Stewart KM, Evans SM, and Morrisey EE. Coordination of heart and lung co-development by a multipotent cardiopulmonary progenitor. *Nature.* 2013;500(7464):589-92.
59. Nishimichi N, Kawashima N, and Yokosaki Y. Epitopes in alpha8beta1 and other RGD-binding integrins delineate classes of integrin-blocking antibodies and major binding loops in alpha subunits. *Sci Rep.* 2015;5(13756.
60. Levitsky KL, Toledo-Aral JJ, Lopez-Barneo J, and Villadiego J. Direct confocal acquisition of fluorescence from X-gal staining on thick tissue sections. *Sci Rep.* 2013;3(2937.
61. Wang C, Zhang J, Fok KL, Tsang LL, Ye M, Liu J, Li F, Zhao AZ, Chan HC, and Chen H. CD147 induces epithelial-to-mesenchymal transition by disassembling CAS/E-cadherin/beta-catenin complex in human endometriosis. *Am J Pathol.* 2018.
62. Satija R, Farrell JA, Gennert D, Schier AF, and Regev A. Spatial reconstruction of single-cell gene expression data. *Nat Biotechnol.* 2015;33(5):495-502.
63. Wu D, and Smyth GK. Camera: a competitive gene set test accounting for inter-gene correlation. *Nucleic Acids Res.* 2012;40(17):e133.

Figure 1. Proximal-distal asymmetry of Hh activation in the adult lung mesenchyme

(**A**) *Gli1*$^{LacZ/+}$ reporter demonstrates *Gli1* expression largely confined to the proximal airway, whereas *Gli2*$^{LacZ/+}$ reporter demonstrates *Gli2* expression both in the proximal airway and distal alveoli. (**B**) Generation of double reporters (*Gli1*$^{LacZ/+}$*:Pdgfra*$^{GFP/+}$ and *Gli2*$^{LacZ/+}$*:Pdgfra*$^{GFP/+}$) demonstrates that GLI1+ cells constitute a significant portion of the PDGFRα+ proximal airway mesenchymal fibroblasts, but does not contribute to the distal mesenchymal fibroblast population. In contrast, GLI2+ cells contribute to both the proximal and distal mesenchyme (arrows, overlap expression). (**C**) Generation of *Gli2*$^{creERT2\text{-}tdT/+}$*:R26R*$^{YFP/+}$*:Ptch1*$^{LacZ/+}$ followed by lineage labeling of GLI2+ cells shows that *Gli2* and *Ptch1* expression largely overlaps in both the proximal and distal mesenchyme. (**D**) Left and Middle: Utilizing fluorescent reporters of *Gli1* and *Gli2* (*Gli1*^{EGFP} and *Gli2*$^{creERT2\text{-}tdT/+}$), we confirm that GLI1+ and GLI2+ cells contribute to a large proportion of the PDGFRα+ mesenchyme in the lung. Right: Crossing the two reporters generates a dual color *Gli1:Gli2* reporter (*Gli1*^{EGFP}*:Gli2*$^{creERT2\text{-}tdT/+}$) which shows that almost all of the GLI1+ cells co-express GLI2, and the GLI2 domain can be divided into a proximal GLI1+ and distal GLI1- subpopulation. (**E**) qPCR analysis demonstrates significant enrichment of Hh target genes *Gli1*, *Ptch1*, and *Ptch2* in the sorted proximal mesenchyme (GLI1+/GLI2+) relative to distal (GLI1-/GLI2+). * $p < 0.05$. Statistical analysis was done using the one tailed Paired Student's t-test. * $p < 0.05$. (**F**) Schematic representing a broad GLI2+ mesenchyme in the adult lung segregated by asymmetric activation of Hh along the proximal-distal axis. Scale bars, 100 μm. Data represent mean ± SEM, with n = 3 per group. Results were replicated (n ≥ 2 experiments).

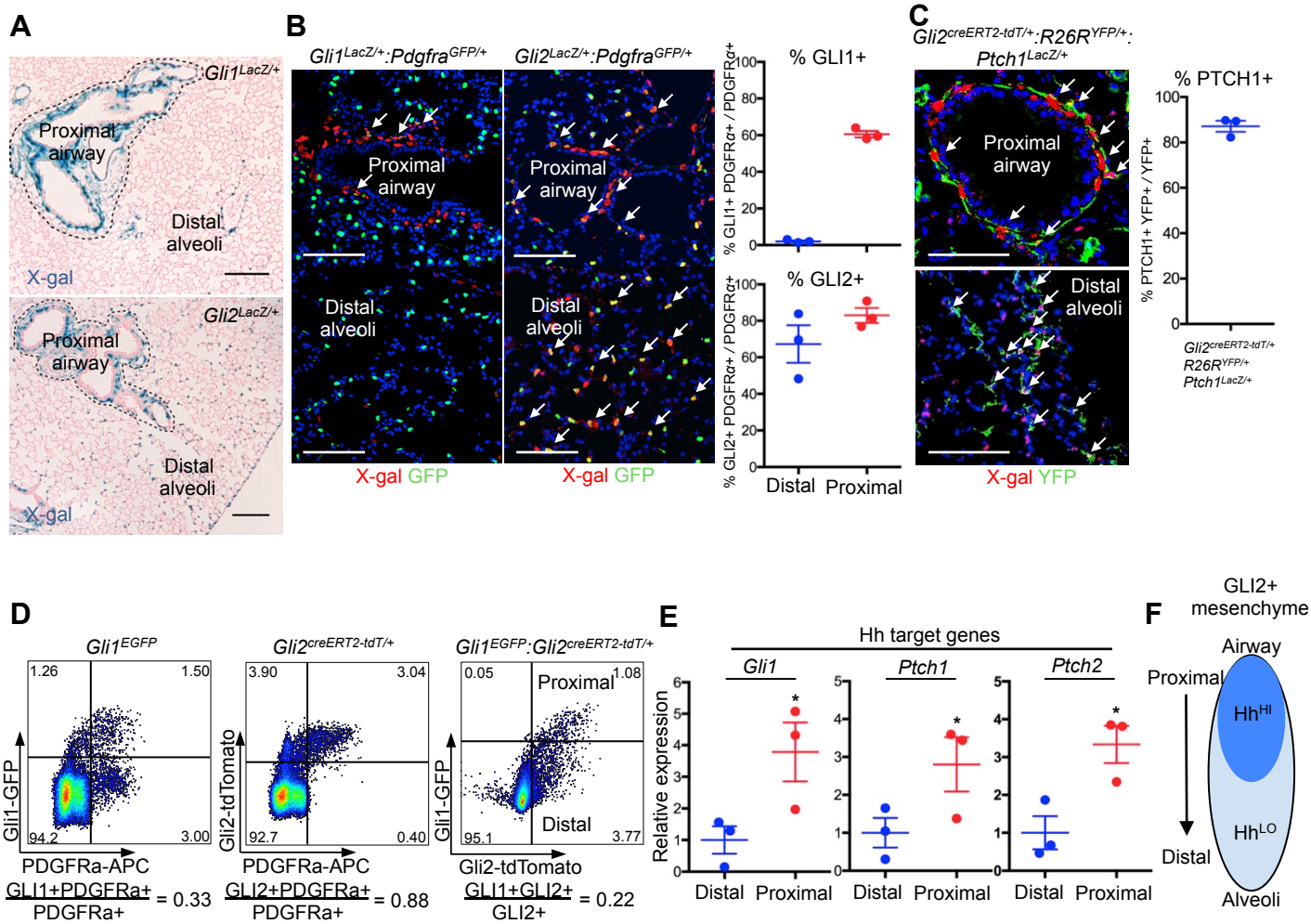
A
Gli1LacZ/+
Proximal airway
Distal alveoli
X-gal
Gli2LacZ/+
Proximal airway
Distal alveoli
X-gal
B
Gli1LacZ/+:PdgfraGFP/+
Gli2LacZ/+:PdgfraGFP/+
Proximal airway
Distal alveoli
X-gal GFP
% GLI1+
% GLI1+ PDGFRα+ / PDGFRα+
% GLI2+
% GLI2+ PDGFRα+ / PDGFRα+
Distal Proximal
C
Gli2creERT2-tdT/+:R26RYFP/+:
Ptch1LacZ/+
Proximal airway
Distal alveoli
X-gal YFP
% PTCH1+
% PTCH1+ YFP+ / YFP+
Gli2creERT2-tdT/+
R26RYFP/+
Ptch1LacZ/+
D
Gli1EGFP
Gli2creERT2-tdT/+
Gli1EGFP:Gli2creERT2-tdT/+
1.26
1.50
94.2
3.00
Gli1-GFP
PDGFRa-APC
GLI1+PDGFRa+ / PDGFRa+ = 0.33
3.90
3.04
92.7
0.40
Gli2-tdTomato
PDGFRa-APC
GLI2+PDGFRa+ / PDGFRa+ = 0.88
0.05
Proximal
1.08
Distal
95.1
3.77
Gli1-GFP
Gli2-tdTomato
GLI1+GLI2+ / GLI2+ = 0.22
E
Hh target genes
Gli1
Ptch1
Ptch2
Relative expression
Distal Proximal
F
GLI2+ mesenchyme
Airway
Proximal
Distal
Alveoli
HhHI
HhLO

Figure 2. Single cell analysis of GLI2+ mesenchyme in the adult lung

(**A**) Unbiased clustering of transcriptomes of individual GLI2+ cells from the adult lung. Each cell is represented as a single dot that is colored by the clustering algorithm and plotted on the tSNE graph. Four distinct clusters emerge from graph-based clustering algorithm with the majority of the cells in Cluster 1 (C1) and Cluster 2 (C2). (**B**) The top expressed genes in Cluster 1 is enriched for GO term "Extracellular Matrix," while the Cluster 2 gene signature is enriched for GO term "Cell-to-Cell Signaling." Size of dot plot represents proportion of cells within the cluster expressing the gene and color denotes level of expression. (**C**) Flow cytometry analysis of the *Gli1:Gli2* reporter (*Gli1*^{EGFP}*:Gli2*$^{creERT2\text{-}tdT/+}$) shows that the Cluster 1 markers, LY6A and LY6C1, detect cells that are predominantly in the Hh^{HI} (GFP+, GLI1+/GLI2+) fraction of the GLI2+ mesenchyme, whereas Cluster 2 marker, ITGA8, detects cells predominantly in the Hh^{LO} (GFP-, GLI1-/GLI2+) fraction. (**D**) Schematic of the experimental flow to isolate GLI2+ cells where the Hh-activation domain is expanded to the distal alveoli for bulk RNA sequencing, with n = 4 per group. (**E**) The mean difference plot displays the log-fold differences (y-axis) versus the mean counts for all genes in the bulk RNAseq experiment, with each dot representing a gene detected in the GLI2+ mesenchyme. The majority of the proximal genes are upregulated in Hh-expanded Gli2+ mesenchyme while the majority of the distal genes are downregulated. Results were replicated (n ≥ 2 experiments).

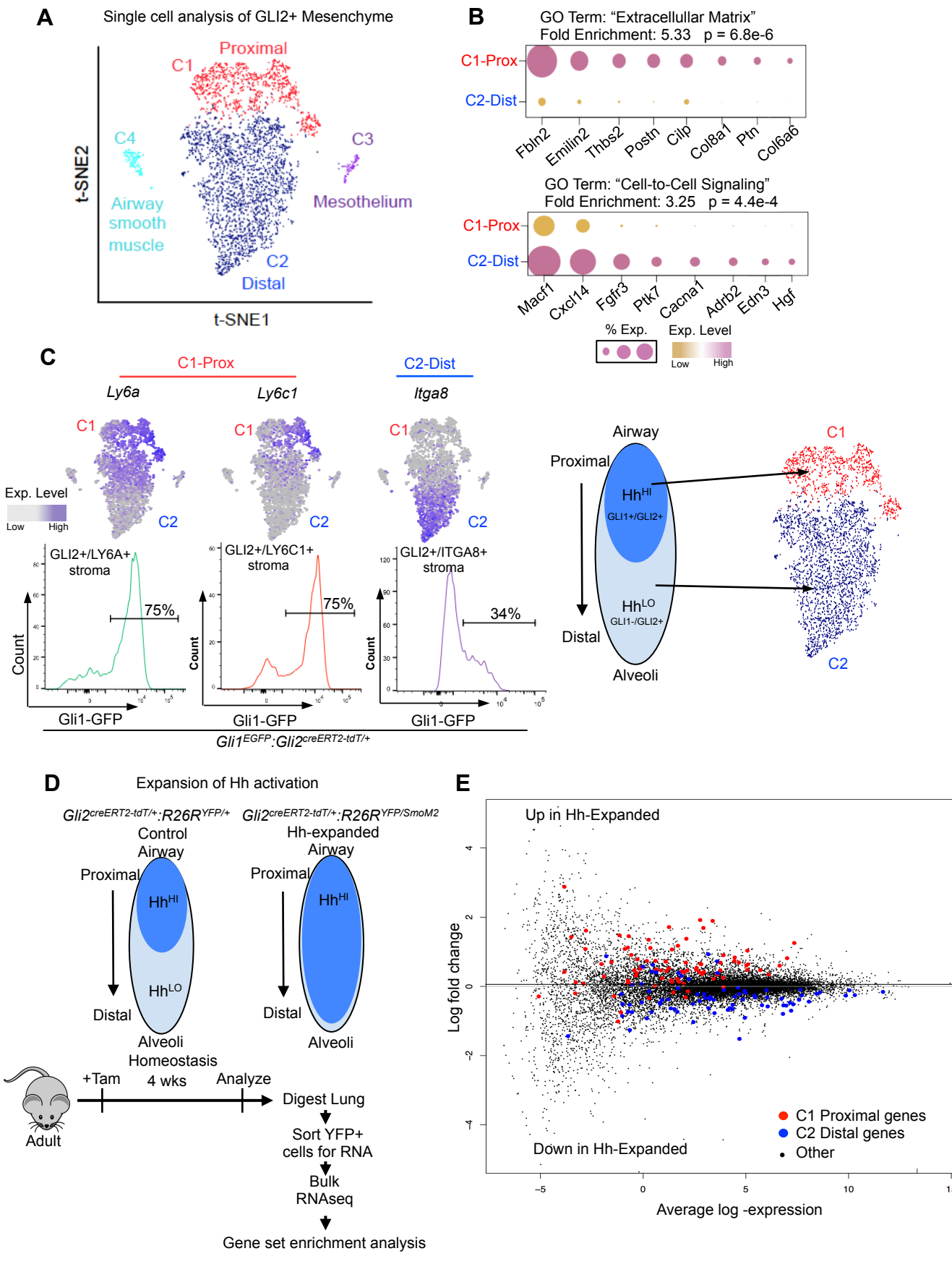
A
Single cell analysis of GLI2+ Mesenchyme
Proximal
C1
C4
C3
Airway smooth muscle
Mesothelium
C2
Distal
t-SNE2
t-SNE1
B
GO Term: "Extracellular Matrix"
Fold Enrichment: 5.33 p = 6.8e-6
C1-Prox
C2-Dist
Fbln2
Emilin2
Thbs2
Postn
Cilp
Col8a1
Ptn
Col6a6
GO Term: "Cell-to-Cell Signaling"
Fold Enrichment: 3.25 p = 4.4e-4
Macf1
Cxcl14
Fgfr3
Ptk7
Cacna1
Adrb2
Edn3
Hgf
% Exp.
Exp. Level
Low
High
C
C1-Prox
C2-Dist
Ly6a
Ly6c1
Itga8
C1
C2
Exp. Level
Low
High
GLI2+/LY6A+ stroma
GLI2+/LY6C1+ stroma
GLI2+/ITGA8+ stroma
75%
75%
34%
Count
Gli1-GFP
Gli1EGFP:Gli2creERT2-tdT/+
Airway
Proximal
HhHI
GLI1+/GLI2+
HhLO
GLI1-/GLI2+
Distal
Alveoli
C1
C2
D
Expansion of Hh activation
Gli2creERT2-tdT/+:R26RYFP/+
Control
Airway
Proximal
HhHI
HhLO
Distal
Alveoli
Gli2creERT2-tdT/+:R26RYFP/SmoM2
Hh-expanded
Airway
Proximal
HhHI
Distal
Alveoli
Homeostasis
Adult
+Tam
4 wks
Analyze
Digest Lung
Sort YFP+ cells for RNA
Bulk RNAseq
Gene set enrichment analysis
E
Up in Hh-Expanded
Down in Hh-Expanded
Log fold change
Average log -expression
C1 Proximal genes
C2 Distal genes
Other

Figure 3. Expansion of Hh activation into the distal mesenchyme induces emphysematous changes

(**A**) Expansion of Hh activation (*Gli2*$^{creERT2\text{-}tdT/+}$*:R26R*$^{YFP/SmoM2}$) into the distal alveoli induced emphysematous changes in the alveolar airspace characterized by increase in mean chord length, enlarged alveolus size, and reduced density of alveoli in the distal compartment. (**B**) Micro-computed tomography (CT) of murine lungs demonstrates increased percentage of low attenuation volume (LAV) as a ratio of the total lung volume (TLV) in Hh-expanded mutants. Dark dots indicate airspace. (**C**) Leukocytes counts in bronchoalveolar lavage fluid (BALF) shows that macrophage is the major composition of leukocytes and there is no significant difference in the number of leukocytes and macrophage of the BALF from both control and Hh-expanded mutants. (**D**) Distal mesenchyme-specific activation of Hh utilizing the *Pdgfra*^{creERT2} allele phenocopied the Hh-expanded mutant (*Gli2*$^{creERT2\text{-}tdT/+}$*:R26R*$^{YFP/SmoM2}$). (**E**) Proximal mesenchyme-specific activation of Hh utilizing the *Gli1*^{creERT2} allele does not induces significant changes in the distal airspace morphology compared to controls. V, blood vessel. Data represent mean ± SEM, with n ≥ 4 per group. Statistical analysis was done using the one tailed Student's t-test. * $p < 0.05$. n.s. not significant. Scale bars: A, D and E, 100 μm; B, 1 mm. Results were replicated (n ≥ 2 experiments).

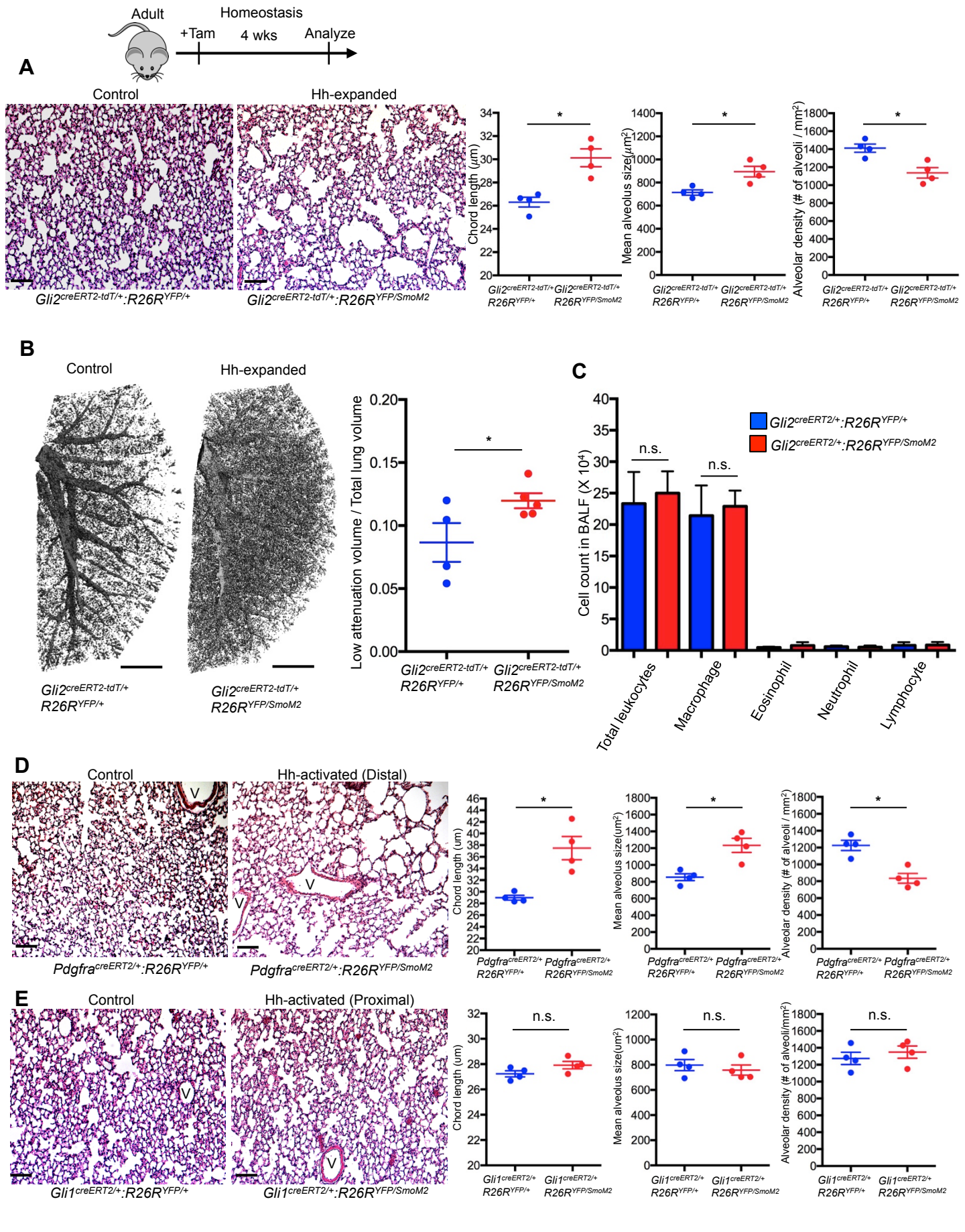
A
Adult
Homeostasis
+Tam
4 wks
Analyze
Control
Hh-expanded
Gli2creERT2-tdT/+:R26RYFP/+
Gli2creERT2-tdT/+:R26RYFP/SmoM2
Chord length (μm)
Mean alveolus size(μm2)
Alveolar density (# of alveoli /mm2)
B
Control
Hh-expanded
Low attenuation volume / Total lung volume
C
Gli2creERT2/+:R26RYFP/+
Gli2creERT2/+:R26RYFP/SmoM2
Cell count in BALF (X 10^4)
n.s.
Total leukocytes
Macrophage
Eosinophil
Neutrophil
Lymphocyte
D
Control
Hh-activated (Distal)
V
Pdgfracreert2/+:R26RYFP/+
Pdgfracreert2/+:R26RYFP/SmoM2
Chord length (um)
Mean alveolus size(um2)
Alveolar density (# of alveoli / mm2)
E
Control
Hh-activated (Proximal)
Gli1creERT2/+:R26RYFP/+
Gli1creERT2/+:R26RYFP/SmoM2

Figure 4. Hh activation in distal mesenchyme reduces proliferation of alveolar stem cells.

(**A**) Expansion of Hh into the distal mesenchyme reduced the number of SFTPC+ stem cells in the alveoli. (**B-D**) Expansion of Hh activation into the distal mesenchyme reduced BrdU incorporation into SFTPC+ alveolar stem cells during normal homeostasis (B) as well as after bleomycin-induced injury (C). Statistical analysis of the percentage of BrdU incorporated SFTPC+ cells (D). (**E**) tSNE plot demonstrates that *Hgf* is enriched in Cluster 2 (bottom cluster) that marks the distal mesenchyme. In situ confirms expression of *Hgf* in the distal mesenchyme. (**F**) SFTPC+ alveolar stem cells express the HGF receptor, MET. Data represent mean ± SEM, with $n \geq 4$ per group. Statistical analysis was done using the one tailed Student's t-test, * $p < 0.05$. Scale bars, 100 μm. Results were replicated ($n \geq 2$ experiments).

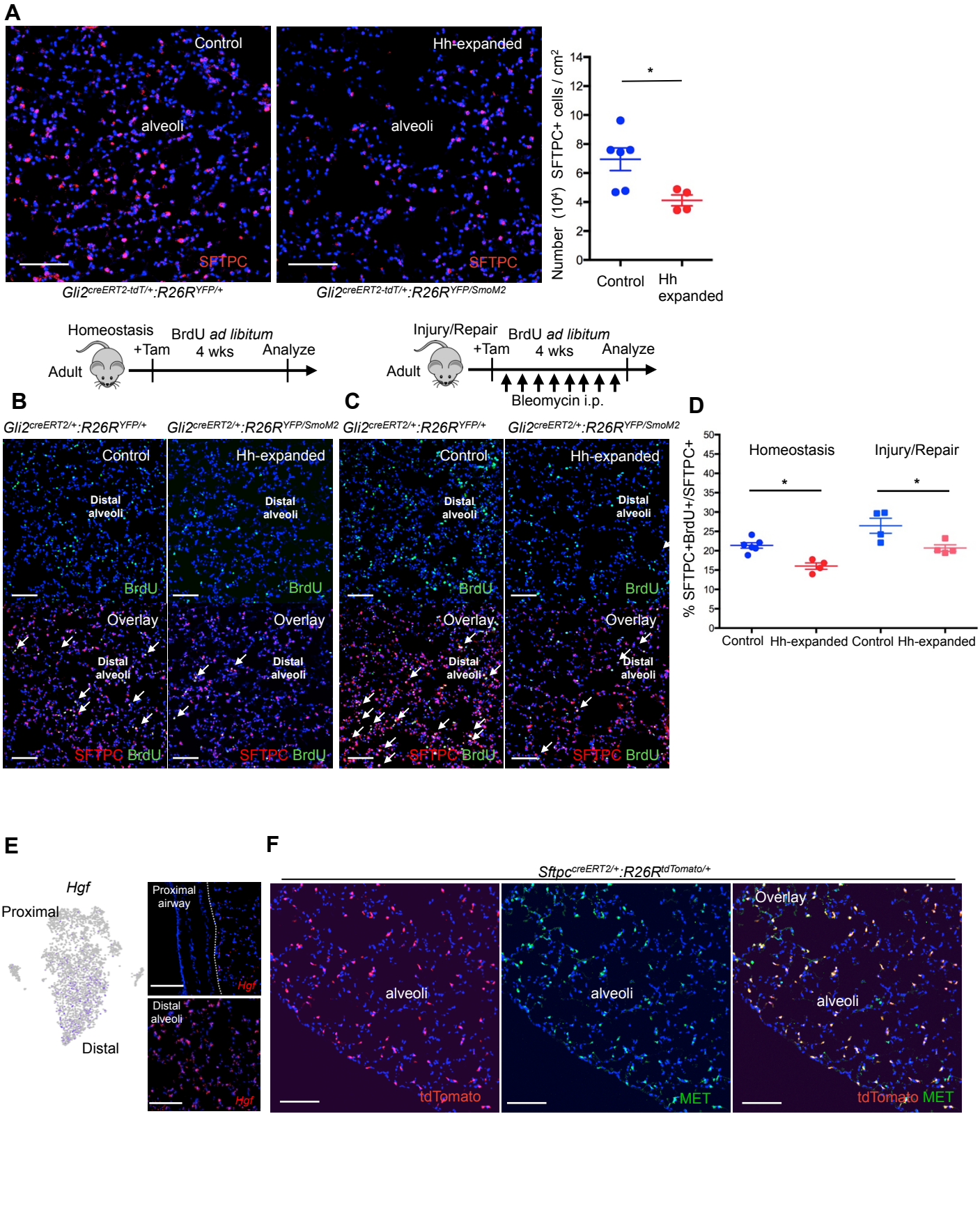
A
Control
alveoli
SFTPC
Hh-expanded
alveoli
SFTPC
Gli2creERT2-tdT/+:R26RYFP/+
Gli2creERT2-tdT/+:R26RYFP/SmoM2
Number (10⁴) SFTPC+ cells / cm²
Control
Hh expanded
Homeostasis
+Tam
BrdU ad libitum
4 wks
Analyze
Adult
Injury/Repair
+Tam
BrdU ad libitum
4 wks
Analyze
Adult
Bleomycin i.p.
B
C
D
Gli2creERT2/+:R26RYFP/+
Gli2creERT2/+:R26RYFP/SmoM2
Control
Hh-expanded
Distal alveoli
BrdU
Overlay
SFTPC BrdU
% SFTPC+BrdU+/SFTPC+
Homeostasis
Injury/Repair
Control
Hh-expanded
E
F
Hgf
Proximal
Distal
Proximal airway
Distal alveoli
Sftpccreert2/+:R26RtdTomato/+
alveoli
tdTomato
MET
Overlay
tdTomato MET

Figure 5. Hh activation disrupts the alveolar niche through suppression of mesenchymal feedback to stem/progenitors.

(**A**) Isolation of lung mesenchymal fibroblasts from *Ubc*$^{creERT2/+}$*:R26R*$^{SmoM2/+}$ animals followed by induction of 4-hydroxytamoxifen (4OHT) activated *Gli1* expression while concurrently downregulating *Hgf* expression. Data represent mean ± SEM, with n = 3 per group. (**B**) SFTPC+ distal alveolar stem/progenitors were co-cultured with Hh-inducible (*Ubc*$^{creERT2/+}$*:R26R*$^{SmoM2/+}$) mesenchyme. 4OHT induction significantly reduced the formation of alveolar organoids, which is partially rescued with the addition of recombinant HGF. Colony forming efficiency = (# of colonies/ # added progenitors) x 100. Data represent mean ± SD, with n = 3 per group. (**C**) Western blotting analysis of phosphorylated MET (pMET), MET and GAPDH in whole lung lysate from Hh-expanded and control mice. Relative protein level of pMET was calculated by pMET/MET. Data represent mean ± SEM, with n ≥ 3 per group. (**D**) Inducible deletion of the HGF receptor, MET, from SFTPC+ alveolar stem/progenitors induced airspace enlargement in the distal compartment of the lung. Data represent mean ± SEM, with n = 5 per group. Scale bars: B, 200 μm; D, 100 μm. V, blood vessel. Each dot represents individual biological replicate. Statistical analysis was done using the one tailed Student's t-test (A, C and D) and one-way ANOVA with Fisher's least significant difference (LSD) test (B). * $p < 0.05$. Results were replicated (n ≥ 2 experiments).

Figure 5. Wang *et al*.

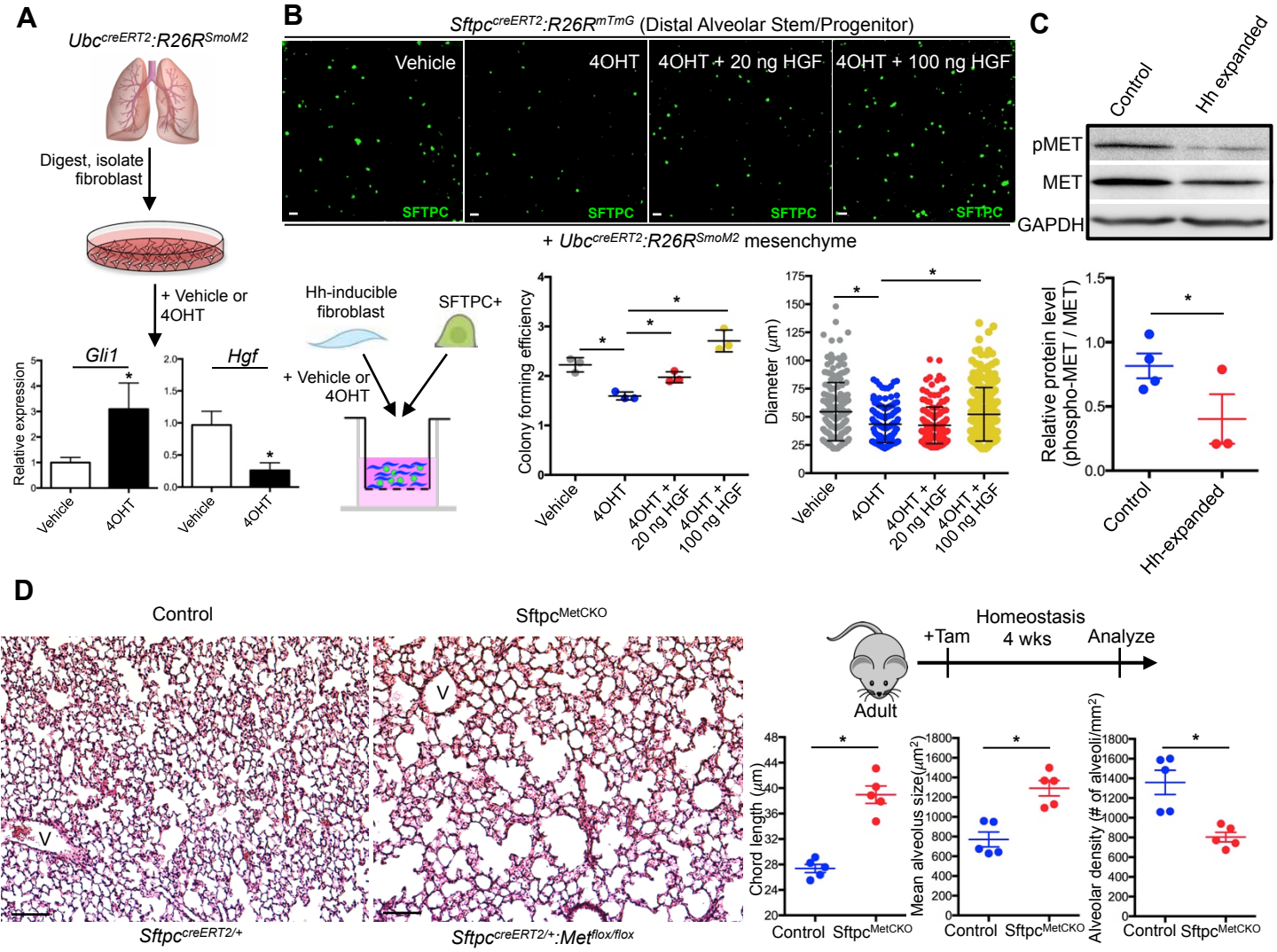

Figure 6. Single cell analysis of the human lung mesenchyme

(**A**) Proximal (enriched in airway) and distal (enriched in alveoli) fragments from the same lung were extracted for separate single cell RNA-sequencing, with the data merged onto the same tSNE projection demonstrating anatomical origin of the cell (each dot represents one cell, red and blue dots are from the proximal and distal fragments respectively). (**B**) Unbiased clustering of individual transcriptomes of the human lung mesenchyme. **(C)** Three distinct subsets emerge from the tSNE projection labeled as Proximal, Distal, and Intermediate. **(D)** The human proximal and distal mesenchymal subset demonstrates significant overlap of homologous genes compared to their murine counterparts. **(E)** Feature plots showing human and murine mesenchymal subsets of comparable anatomic localization have similar enriched genes (feature dot plots of murine *Itga8, Thy1, Npnt, and Fbln2* appeared in Fig. 2C and Supplemental Figure 2C). (**F**) The top expressed genes in the proximal subset is enriched for GO term “Extracellular Matrix,” while the distal gene signature is enriched for GO term “Cell Communication.” Size of dot plot represents proportion of cells within the cluster expressing the gene and color denotes level of expression. (**G**) qPCR analysis of the sorted proximal (THY1+) and distal mesenchyme (ITGA8+) demonstrates enrichment of Hh target genes *GLI1*, *PTCH1*, and *PTCH2* in the proximal mesenchyme relative to distal mesenchyme. Data represent mean ± SEM, with n = 3 per group. Statistical analysis was done using the one tailed Student’s t-test. * $p < 0.05$. (**H**) Schematic representing human lung mesenchyme segregated by asymmetric activation of Hh along the proximal-distal axis. Results were replicated (n ≥ 2 experiments).

Figure 6. Wang *et al*.

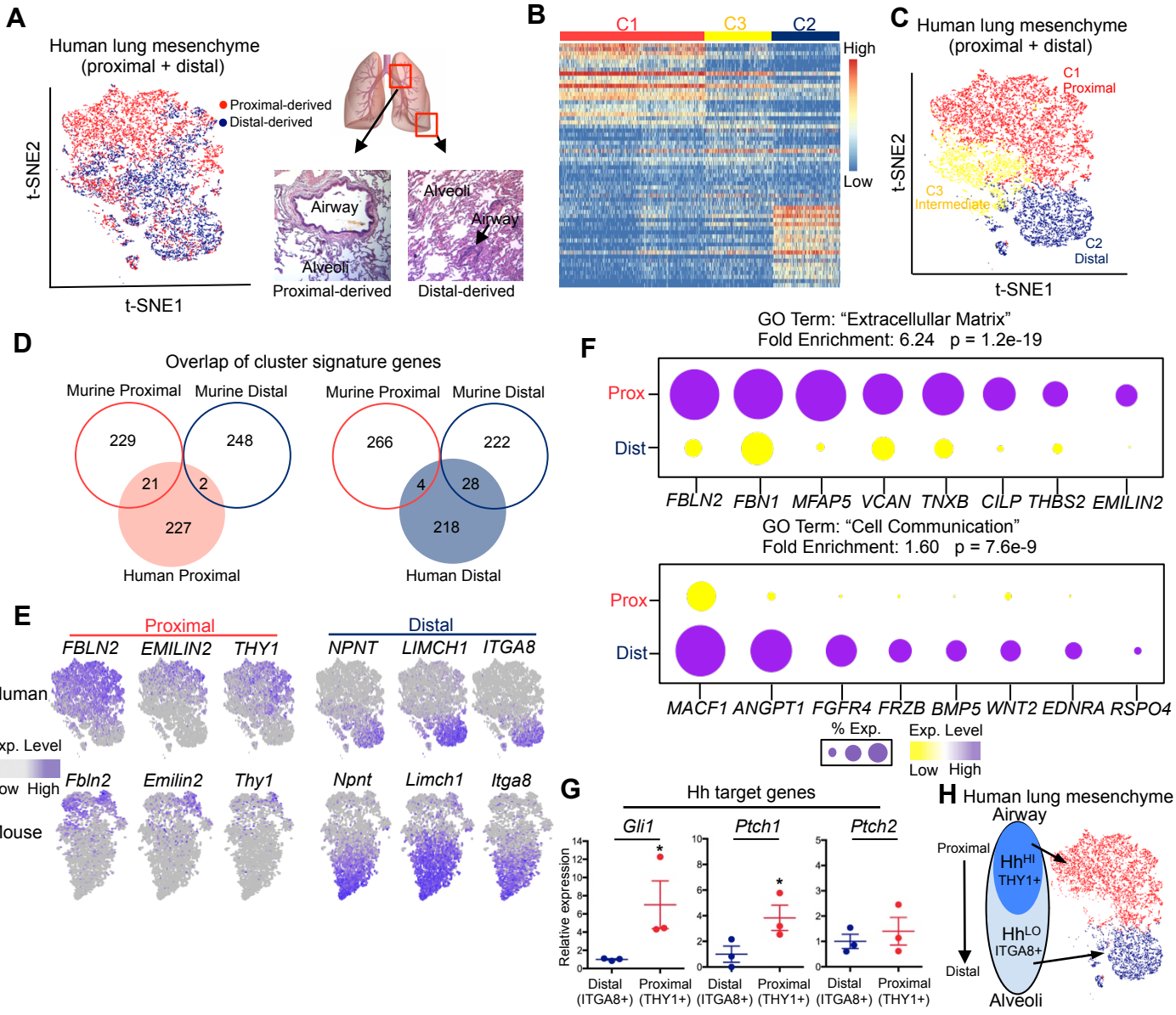

Figure 7. Model of Hh asymmetry regulating discrete mesenchymal identities.

(**A**) Model of Hh asymmetry maintaining distinct proximal-distal mesenchymal identities and (B) ectopic Hh activation disrupting distal mesenchymal identity and the alveolar stem cell niche.

Figure 7. Wang *et al*.